IEEE *Access*
Multidisciplinary : Rapid Review : Open Access Journal

RESEARCH ARTICLE

Latency Analysis for Real-Time Sensor Sharing Using 4G/5G C-V2X Uu Interfaces

SINUK CHOI, DONGYOON KWON[ID], AND JI-WOONG CHOI[ID], (Senior Member, IEEE)

Department of Electrical Engineering and Computer Science, Daegu Gyeongbuk Institute of Science and Technology (DGIST), Daegu 42988, Republic of Korea

Corresponding author: Ji-Woong Choi (jwchoi@dgist.ac.kr)

ABSTRACT With the development of communications, various applications of communication technologies, such as remote driving, delivery drones, and telesurgery, are emerging. In particular, in many cases, these applications need real-time video transmission services, and they should support low latency for operation reliability and quick response in emergencies. Sensor sharing is required to support advanced communication services, but the latency analysis of device-to-remote users or remote servers with high data traffic is insufficient. Most related works have device-to-device communication or low data traffic messages for basic device status sharing. However, the latency analysis of sensor sharing between a device and a remote server or remote user is essential to support advanced communication services such as autonomous driving utilizing data offloading and device operation by remote users via the base station and server. Therefore, in this paper, we analyze the end-to-end latency and latency elements for video sharing, which is the most representative sensor in 4G long-term evolution (LTE) and 5G new radio (NR) Uu interfaces. In addition, we derive the supportable video resolution according to the raw video and encoded video transmission in each communication system. For each video resolution level, we analyze which latency elements have a significant effect on the end-to-end latency. Depending on each communication system, we investigate the number of users for the real-time sensor-sharing system that can be supported at the same time. Simulation results show that the LTE Uu interface supports up to full high definition (FHD) video resolution, and the 5G Uu interface supports up to ultrahigh definition (UHD). Additionally, the results show that only a single user can be supported with the FHD resolution level in the LTE Uu interface, whereas up to 19 users can be supported in the 5G Uu interface.

INDEX TERMS Remote driving, sensor sharing, cellular communication system, end-to-end latency, vehicle-to-everything, cellular network latency.

I. INTRODUCTION

As communication technology develops, various applications such as drone delivery, smart manufacturing, vehicle-to-everything (V2X), remote surgery, and connected health care are emerging. These applications are considered future core business items in various fields, such as telecommunications, electronics, and traditional automotive manufacturers [1], [2]. Among various communication applications, V2X is considered one of the most representative business models

The associate editor coordinating the review of this manuscript and approving it for publication was Jie Gao[ID].

because it can be used for various services, such as advanced autonomous driving, remote driving services, and robotaxis [3]. These services allow businesses to secure loyal customers and ongoing revenue. Therefore, many researchers have studied implementing V2X communication application services in a realistic environment.

The V2X system requires robust communication with low latency because users and operating systems should be capable of real-time surroundings recognition and emergency response. During driving, to be aware of real-time road information, vehicles and roadside units (RSU) share vehicle and road environment data such as adjacent vehicle

information, traffic light information, pedestrian locations, etc. To support V2X services, cellular V2X communication (C-V2X) and dedicated short-range communication (DSRC) are considered representative communication technologies for supporting intelligent transportation systems.

DSRC is based on 802.11p wireless fidelity (Wi-Fi) technology and has no communication cost except for device installation, but it has a low data rate, limited network connectivity, and short communication coverage [4], [5]. In addition, IEEE 802.11 bd is defined to reduce the performance gap between DSRC and C-V2X and improve communication performance such as latency and reliability [6]. C-V2X is based on general cellular communication technology such as long-term evolution (LTE) and 5G new radio (NR). Therefore, it has merit for network connectivity and broad communication coverage between the vehicle and the base station compared to DSRC. 3GPP defined two modes of communication operation: the PC5 interface for direct communication and the Uu interface for vehicle-to-network communication [7]. PC5 interfaces provide sidelink communication between vehicle-to-vehicle communication and vehicle-to-RSU communication, which allows lower communication latency compared to the conventional cellular communication system [8], [9]. By using the PC5 interface, a vehicle can share its status report and driving condition with a nearby vehicle or RSU and receive traffic information on the adjacent road from the RSU. Uu interfaces offer vehicle network connectivity between the vehicle and server. In addition, they can communicate with vehicles in other cities or users. Thus, a service provider can support infotainment service, vehicle status reports, route control messages from the servers, and traffic warnings on the vehicle's route from a distant road via the Uu interface. There are key performance indicators (KPIs) for V2X services, such as latency, communication reliability, power consumption, and system throughput. Among these KPIs, one of the most important KPIs in V2X is latency because low latency is paramount to offering vehicle status sharing and emergency alerts. Additionally, in advanced driving and remote driving, which are the representative use cases of V2X as defined by the 3rd generation partnership project (3GPP), low latency is essential [10].

To date, many researchers have researched and analyzed the communication performance of the C-V2X PC5 interface or DSRC V2X communication system or messages with periodic low data rates, such as cooperative awareness messages (CAMs) and basic safety messages (BSMs) [11]. These communication systems could be used for vehicle communication implementation or basic vehicle status sharing because of less network connectivity and low data rates [12], [13]. Unlike the PC5 interface or DSRC, there has been little analysis and research on Uu interfaces and messages with a high data rate to support sensor sharing and data offloading. However, Uu interfaces become more important as the level of automation increases and as operators are about to provide higher-level applications since it can offer

network connections with automated processing servers or remote users.

Therefore, researching Uu interfaces with high data rate messages such as video and vehicle sensor messages is essential for supporting future vehicular applications such as remote driving, see-through for path maneuvers, and vehicle sensor sharing [10], [14]. In particular, these applications need low-latency communication, and service providers should satisfy service within the latency threshold. However, end-to-end latency and the latency elements for real-time high data traffic, such as sensor data on the C-V2X Uu interface, have not yet been analyzed. If the system provides high-level resolution sensor data, the remotely located user can utilize data more precisely. However, when the vehicle transmits high-level resolution data, the system needs to support wider bandwidth and requires more time to transmit. In addition, more retransmission processes will occur, such as hybrid automatic repeat requests (HARQs). As a result, the end-to-end communication latency increases with the sensor resolution level. Thus, we investigate the end-to-end latency and latency elements affecting the end-to-end latency according to sensor resolution and compression.

In this paper, we determine the end-to-end latency and each latency element of the real-time sensor-sharing system on the C-V2X Uu interface. Among the sensor data of the vehicle, we assume that the vehicle shares its video camera data because the video is the representative sensor data on autonomous driving and the V2X system. Thus, we analyze the latency performance according to the video resolution level and compression level on the LTE and 5G Uu interface. To evaluate whether video resolution is supportable, we investigate the interframe latency of the video-sharing system and frame per second (fps) threshold.

The remaining parts of this paper are organized as follows. In Section II, we briefly review the previous studies. In Section III, we describe the end-to-end latency model and latency elements that constitute the end-to-end latency. In Section IV, we describe the end-to-end latency simulation results according to video resolution and video encoding in LTE and 5G communication networks. Finally, conclusions are drawn in Section V.

II. RELATED WORK

Latency analysis and research have been conducted in various ways for V2X and real-time applications. Representatively, researchers conducted end-to-end latency measurements through communication system implementation, and they analyzed the latency and performed simulations through V2X message transmission with a low data rate.

In latency measurements through communication system implementation, measurements were conducted with the driving platform or with the communication module in a realistic application environment. Moto et al. in [15] worked on a truck platooning field trial system for vehicle-

to-network (V2N) communications using 5G prototype equipment using four trucks, and they measured the channel path loss and round trip time (RTT) latency. In the research conducted in [16], the authors constructed a 1/10 scale vehicle test platform for the remote driving test, and the test participants drove using the built platform via Wi-Fi. To apply LTE latency to their platform, the authors measured the commercial LTE cellular network latency. The authors in [17] measured LTE latency over four mobile carriers for latency-sensitive mobile applications such as mobile virtual reality services and multiplayer mobile games. Reference [18] presented the glass-to-glass, timestamp-based latency for different camera configurations and encoder settings. End-to-end latency measurement through implementation is essential for supporting a variety of communication applications. However, to reduce the end-to-end latency, it is also important to identify which latency element has a dominant effect on the end-to-end latency of each application.

Additionally, latency analyses of the V2X system have been actively studied. The authors in [19] and [20] introduced the end-to-end latency model of V2N on the 5G communication system and estimated the end-to-end latency with an 800-byte packet. The work done in [21] proposed a latency analysis model of C-V2X systems by dividing the V2X latency into transmission time interval (TTI) independent latency and TTI proportional latency on V2X, evaluating the latency of V2X systems and simulating a sidelink V2X system considering low packet size. Reference [22] shows the performance of a cellular communication system when the device transmits periodic 100-bit messages with a 10 ms interarrival time under various design features, as in the scheduling method and TTI. The research conducted in [23] measured the download latency of high-definition maps with high data rates for the V2X system. There were many analyses of the end-to-end latency and latency elements, but most of the studies presented the results with low-volume data or periodic vehicle status messages. However, to support advanced application services, latency analysis of messages with a high data rate or sensor data is essential.

The main contribution of our paper is to present the end-to-end latency of data transmission and derive latency elements with a high data rate occurring in the C-V2X Uu interface. We assumed a real-time video-sharing system because video sensor data have a high data rate and are representative and important for providing advanced communication application services. We model the end-to-end latency in LTE and 5G C-V2X Uu interfaces and show the simulation results and supportable video resolution according to video encoding and the number of users.

III. SYSTEM MODEL
As shown in Fig. 1, we assume that the vehicle transmits a real-time driving video to a driving operator such as a remote

user or a central mobile server. Additionally, the vehicle can change the video resolution and the encoding level depending on the channel state or the user's request. For example, when the driver is remotely located and drives the vehicle for logistics transportation or to pick up the passenger, the driver should receive a real-time driving video to drive safely in the real road environment. Additionally, if the artificial intelligence system that is located on the remote server controls the vehicle through offloading, realistic driving video is indispensable. In this scenario, we analyze the end-to-end latency and the latency elements in the video-sharing system.

To analyze which latency element dominantly affects the total latency, we define the total latency of each video frame, L_T, which is expressed as

$$L_T = L_{seg} + L_{enc} + L_{retrans} + L_{net} + L_{etc}, \quad (1)$$

- L_{seg} is the segmentation latency, which is the time it takes to transmit to the end of the segmented traffic of the video frame. When the traffic of the video frame is too large to transmit in a single TTI unit despite using the entire physical resource, the transmitter should transmit whole video data through several TTI units by segmentation because of the payload limit. L_{seg} is affected by the data traffic of the video frame and the transport block size. Therefore, L_{seg} is defined as

$$L_{seg} = \frac{N_{video}}{N_{TBS}}, \quad (2)$$

where N_{video} is the data traffic of each video frame, which varies according to video resolution, color depth, encoding method, etc. N_{TBS} is the transport block size of the communication system, which is determined by the communication environment, parameter configuration, and device capability.

- L_{enc} is the video encoding processing latency, which is the time it takes to convert the raw video to the desired format and traffic size. L_{enc} will be 0 when the system uses raw video. By using video encoding, raw video data traffic is reduced while maintaining video quality. The encoding time can differ by encoding format, such as moving pictures experts group 1 (MPEG-1), advanced video coding (AVC), alliance for open media video 1 (AV1), etc.

- $L_{retrans}$ is the retransmission latency, which represents the HARQ retransmission processing time between the transmitter and receiver on the wireless communication channel. Due to cellular communication characteristics, the receiver uses a cyclic redundancy check (CRC) to check bits of received data to determine error occurrence. When a communication error occurs, the receiver should request data retransmission. Therefore, the receiver sends a negative acknowledgment (NACK) to the transmitter, and it receives the retransmitted signal from the transmitter. In this process, the receiver can
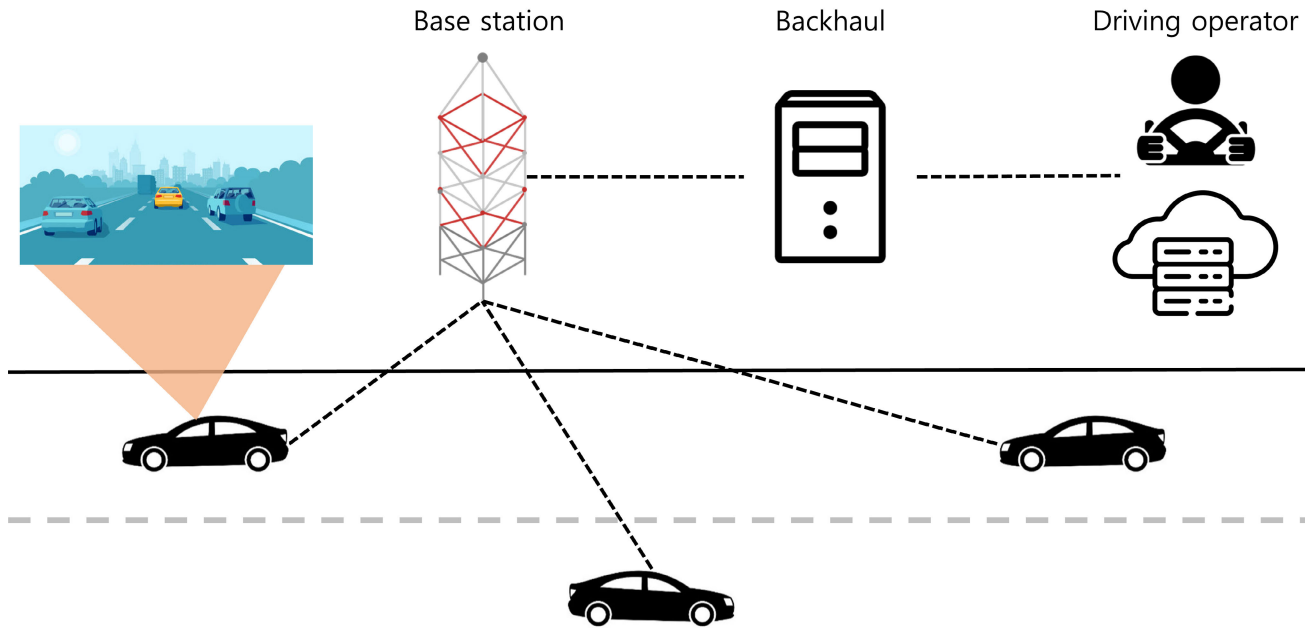
FIGURE 1. The end-to-end latency per frame of the raw video of the single user on the Uu interface.

improve reliability, but retransmission inevitably occurs with additive communication latency. $L_{retrans}$ can be decomposed as

$$L_{retrans} = N(L_{BS,HARQ} + L_{NACK} \\ + L_{UE,HARQ} + L_{RT}), \quad (3)$$

where N is the number of retransmissions and $L_{BS,HARQ}$ represents the latency at the base station, which includes the data decoding time, demodulation time, NACK message preparation time, etc. L_{NACK} is the duration of NACK message transmission. $L_{UE,HARQ}$ is the latency at the device, which includes the process of receiving and decoding a NACK message, generating a retransmission packet, and so on. Finally, L_{RT} means the duration of retransmitted data.

- L_{net} is the network processing latency. L_{net} includes the processing time in backhaul, which consists of the serving gateway (S-GW), packet data network gateway (PDN gateway, P-GW), etc. After the base station decodes the transmitted data in the air successfully, the decoded data are routed and delivered from the base station to a remote user or mobile server. In this process, the backbone network intermediate links between the base station and the network, and additional latency occurs. In this paper, L_{net} follows the network latency that is defined in [24] and [25].

- L_{etc} includes the time that processes bit modulation, channel encoding on the transmitter (L_{mod}), data decoding, demodulation time on the base station (L_{BS}), and air propagation time (L_{air}) under the wireless communication system.

IV. SIMULATION RESULTS AND ANALYSIS

In this section, we analyze L_T on the LTE and 5G communication Uu interface system and investigate whether a real-time video transmission service could be supported when the system provides the maximum payload. In the Uu interface environment, it may be difficult to support the maximum payload due to characteristics such as the fast-moving speed of the vehicle. However, since there were no integrated latency performance guidelines that could be supported maximum in each system, it is necessary to present guidelines for maximum achievable performance depending on each system and image resolution. Based on the guidelines, service providers can predict the supportable sensor resolution, compression, number of users, etc. that can be considered when designing a system. Also, the latency performance analysis can give an intuition as to which latency elements should be reduced to improve end-to-end latency performance effectively. Therefore, we assume that each communication system supports the maximum bandwidth size. That is, we assume that the service provider allocates the entire frequency band for the real-time image transmission service to support the maximum bandwidth size. Additionally, it is assumed that the bandwidth is limited to half the maximum bandwidth considering other cellular communication services and the real-time video-sharing service are simultaneously supported. In other words, it utilizes a maximum number of physical resource blocks and uses the highest modulation scheme on each communication system, implying a lower bound of L_T.

To decide whether the communication system can support each video resolution, we analyze whether L_T satisfies the latency threshold condition. The latency threshold varies

according to the fps of the video configuration. We assume that remote users receive each video frame within at least a video frame generation period to perform real-time judgment and control. In this simulation, each video provides 30 fps, and the color depth of the video frame is 16 bits, which is the number of bits used to represent the different colors of each pixel. We assume that N_{video} of bit-converted raw video, $N_{video,Raw}$ is

$$N_{video,Raw} = R_h R_v D, \qquad (4)$$

where R_h and R_v indicate the number of horizontal and vertical pixels of each video frame, according to the video quality, respectively, and D is the color depth.

As mentioned in section III, L_{enc} only adds to L_T when the video is encoded to reduce the data traffic. In this paper, we fix the encoding format to be H.264 AVC, which is a broadly used standard encoding format even today [26]. H.264 AVC has merits in compression rate with tolerable process complexity compared to MPEG, and subsequent encoding formats of the H.264 such as H.265 and H.266 provide small performance improvements for very large algorithmic complexity. Defining and quantifying the video encoding latency is difficult because it depends on various parameters, such as frame-to-frame variation, encoding set, and key-frame period. Likewise, the encoded data traffic for each video frame varies according to the parameter configuration and frame characteristics. Therefore, we set the encoding level of H.264 as 6, and the encoding speed, v_{enc} and encoded data traffic of the video frame, $N_{video,Enc}$ follows the maximum decoding speed and data traffic, which are defined in [27]. v_{enc} is the macroblock processing rate per second, which is the processing unit of the video compression format based on a linear block transform. Thus, the encoding latency for each video frame, L_{enc}, is

$$L_{enc} = \frac{R_h R_v}{M^2 v_{enc}}. \qquad (5)$$

where M is the unit sample size of macroblock [28].

A. 4G LTE

First, we analyze the end-to-end latency and latency elements of each video frame of bit-converted raw video and encoded video under a 4G cellular communication system. Additionally, the end-to-end latency performance according to the number of users is analyzed. We assume that the bandwidth of the system is 20 MHz and the modulation scheme is 64 quadrature amplitude modulation (QAM), which is the highest modulation order supported in the LTE system, and turbo code is adopted for channel coding [29]. Other parameter configurations used in 4G LTE and 5G NR simulations are described in Table 1. In 3GPP, the block error rate (BLER) threshold for the selected modulation and coding scheme (MCS) index is set as 10%. Most communication vendors generally set the minimum BLER threshold at 10% to prevent excessive network congestion. Therefore,

TABLE 1. Simulation parameter configuration.

Parameters	4G LTE	5G NR
Subcarrier spacing	15 kHz	60 kHz
Modulation order	64 QAM	256 QAM
Bandwidth	20 MHz	100 MHz
Channel coding	Turbo code	LDPC code
TTI duration	1 ms	0.25 ms
Code rate	0.8333	0.9258
Channel model	CDL channel	
Noise figure	5 dB	
Thermal noise	-101 dBm	

we assume that the real-time video-sharing system satisfies the minimum BLER of 10% to satisfy the minimum operating condition for the selected MCS index [30]. Additionally, we assume that the generated waveform passes through a Rayleigh fading channel, and zero-mean additive white Gaussian noise (AWGN) is added to the passed waveform. The used fading channel model is a broadly used clustered delay line (CDL) model defined for link-level simulation evaluation in the frequency band from 0.5 GHz to 100 GHz in the 3GPP standard [31]. In this simulation, we refer to the standard that presents the evaluation method and parameter configuration for V2X use cases in LTE and 5G systems to describe the V2X communication environment and scenario of vehicles. Detailed channel model settings follows Table 6.2.3.1-4 which presents V2X channels in the urban highway environment in [32]. If an error occurs, the receiver notices it because the receiver always checks CRC bits to determine an error due to the communication channel and noise in the received data. In the simulations, we build a transceiver and fading channel based on the LTE Toolbox and Communications Toolbox in MATLAB 2020a and the simulations are run on Intel i7 8700K CPU running at 3.70 GHz with NVIDIA GeForce GTX 1080 GPU.

The transport block size of the LTE system per TTI, $N_{TBS,4G}$ can be approximately described as

$$N_{TBS,4G} = N_{Slot} N_{SC}^{RB} N_{Symb} Q_m N_{RB} - N_{RS} - N_{OH}, \qquad (6)$$

where N_{Slot} expresses the number of slots per transmission unit, N_{SC}^{RB} indicates the number of resource elements (REs) per resource block, N_{Symb} is the number of symbols per slot, N_{RS} is the data traffic of the reference signal, Q_m is a modulation order, N_{RB} is the number of resource blocks, and N_{OH} is the overhead data traffic size, which includes a primary synchronization signal (PSS), a secondary synchronization signal (SSS), etc. Additionally, in the LTE system, an accurate $N_{TBS,4G}$ is represented by a table according to N_{PRB}, Q_m, and the modulation and coding scheme (MCS) index [30]. Therefore, $L_{seg,4G}$ can be represented by

$$L_{seg,4G} = \lceil \frac{N_{video}}{N_{TBS,4G}} \rceil, \qquad (7)$$

where $\lceil \cdot \rceil$ is the ceiling function. In addition, in $L_{retrans}$ of the LTE system, $L_{retrans,4G}$, $L_{BS,HARQ}$ and $L_{UE,HARQ}$ spend 3 TTIs, as in [33]. L_{NACK} and L_{RT} have 1 TTI since
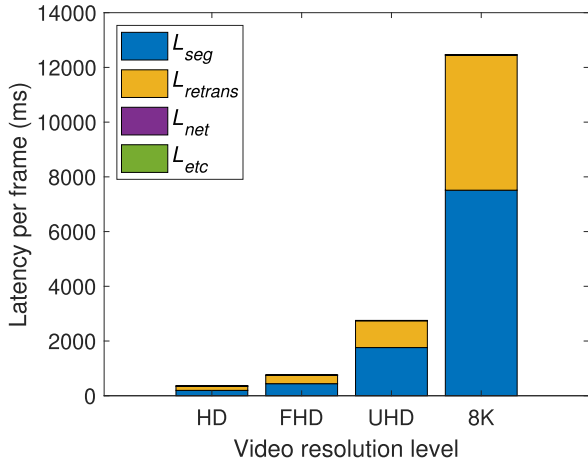
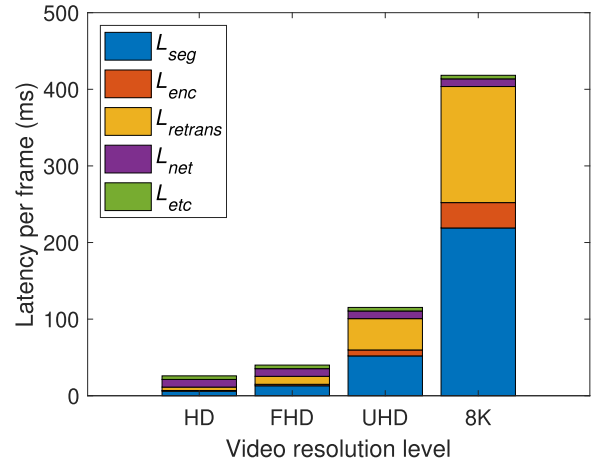**FIGURE 2.** The end-to-end latency per frame of the raw video of the single user on the LTE system.

FIGURE 3. The end-to-end latency per frame of the encoded video of the single user on the LTE system.

FIGURE 4. The end-to-end latency per frame of the encoded FHD video of the single user on the LTE system with 50% background traffic.
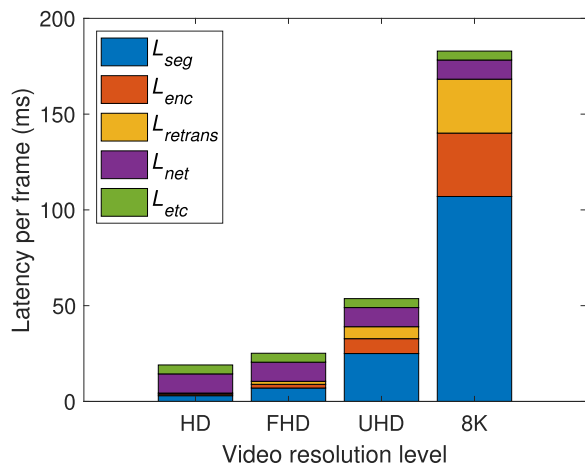
transmission time compared to lower video resolution because of restricted data throughput. Thus, L_{seg} inevitably increases compared to low video resolution. Additionally, $L_{retrans}$ increases because message retransmissions rise as the number of transmissions per video frame increases. In the raw video transmission, the remaining latency elements except for L_{seg} and $L_{retrans}$ have little effect on L_T at all video resolutions.

Fig. 3 shows the end-to-end latency of the encoded video of the single user on the LTE system. Unlike L_T of the raw video, L_{enc} is added to L_T because an additional delay inevitably occurs to encode and compress the raw video. We assume that the raw video is encoded by using H.264 AVC, level 6. Similar to Figure 2, in Figure 3, L_T increases with video resolution. Although the data traffic is reduced by encoding the raw video, it still has plenty of data traffic depending on the resolution of the raw video. Unlike L_T of the raw video, the real-time video transmission of HD and FHD resolution can be supported under the LTE system because L_T satisfies the latency threshold, i.e., 33.3 ms. However, at high video resolutions, UHD and 8K cannot be supported despite video encoding. At lower video resolutions, the encoded video has low data traffic per video frame. Therefore, L_{seg} and L_{enc} affect L_T less in HD and FHD video, and the other latency elements, L_{net} and L_{etc}, are more dominant on L_T. However, at high resolution, L_{seg} and $L_{retrans}$ are dominant in L_T, similar to raw video, because data traffic is still too large to support real-time video transmission. Therefore, L_T on UHD and 8K video resolution cannot satisfy the latency threshold condition.

Fig. 4 shows the end-to-end latency per frame of the encoded video of the single user on the LTE system with 50% background traffic. In the case of bandwidth, the figure was derived when bandwidth for V2X and bandwidth for general users were divided and allocated due to use of communication services by other users such as pedestrians or vehicle passengers. Thus, in Fig. 4, we assume that the background
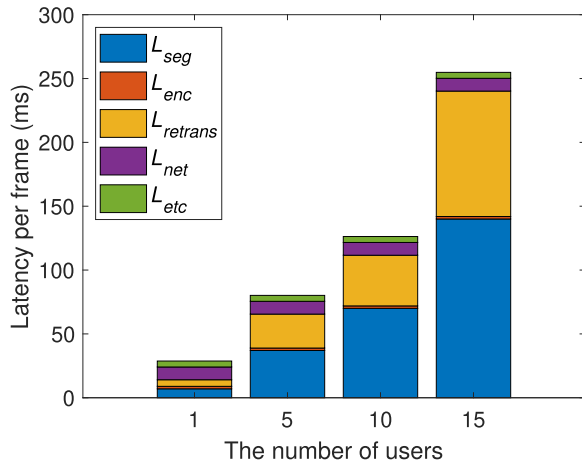
they spend the time duration during data transmission [33]. Therefore, in the LTE system, 8 TTIs are taken per retransmission trial.

Fig. 2 presents the end-to-end latency per frame of the raw video of the single user for a given video resolution on the LTE system. We considered four video resolutions: high definition (HD), full high definition (FHD), ultrahigh definition (UHD), and 8K UHD (8K). For each resolution, each frame consists of 1280 by 720 pixels for HD, 1920 by 1080 for FHD, 3840 by 2160 for UHD, and 8192 by 4320 for 8K. In this figure, L_{enc} is disregarded since the raw video is not encoded. Under every video resolution, the L_T of the real-time video-sharing system cannot satisfy the latency threshold (33.3 ms) since the data traffic of the raw video is too large to transmit via the LTE system. Therefore, it cannot support real-time transmission. As video resolution increases, both L_{seg} and $L_{retrans}$ increase and predominantly affect L_T. Since the data traffic rises with video resolution, the transmitter should transmit video frames with a longer

FIGURE 5. The end-to-end latency according to the number of users of encoded FHD video on the LTE system.

traffic generated by the general communication service users can only allocate about 50% of the physical resources to the vehicle in a real-time sensor-sharing system. Compared with Fig. 3, the end-to-end latency performance was degraded under all resolution conditions because L_{seg} and $L_{retrans}$ increased due to limited physical resources. In addition, in the absence of background traffic, the service provider was able to support FHD resolution in the LTE system. However, if background traffic exists, it can only support up to HD resolution due to degraded latency performance.

Fig. 5 illustrates the end-to-end latency of the encoded FHD video according to the number of users on the LTE system. When a single user uses the real-time video-sharing service, FHD resolution video is supportable, as shown in Fig. 3. However, if multiple users use the real-time video-sharing service simultaneously, the service with FHD resolution cannot be supported because the transmitter spends more time transmitting the same video frame compared to a single user. Since the users share limited physical resources, the available physical resources per user decrease. Thus, as the number of users increases, L_{seg} inevitably increases. Additionally, at high resolution levels, the impact of $L_{retrans}$ is greater because the number of retransmissions increases as the segmentation of each video frame increases, and each retransmission introduces an additional 8 ms of latency in the LTE systems. Consequently, real-time video transmission services in the LTE system can support only one user with FHD resolution. Since the real-time video-sharing service requires a high data rate, the number of users that can be supported is limited. Therefore, it is only available to a limited number of vehicles. If a service provider wants to support more users in the LTE system, a video with a low resolution should be provided or larger bandwidth should be supported.

B. 5G NR
Similar to the above subsection, we investigate the end-to-end latency and latency elements of each video frame of

raw video and encoded video under the 5G NR system. In addition, we present the end-to-end latency according to the number of users. In the 5G system, we assume that the bandwidth is 100 MHz, the modulation is 256QAM, which is a higher modulation order in the 5G system, and low-density parity check coding (LDPC) is used for channel coding [34]. Additionally, as in the LTE system, the generated waveform passes through the Rayleigh fading channel, whose model is the TDL model, and AWGN is added to the passed waveform. The real-time video-sharing system satisfies the BLER threshold to satisfy the minimum operating condition for the selected MCS index. The transceiver and fading channel are built based on the 5G Toolbox and Communications Toolbox in MATLAB 2020a.

The TTI length in the 5G system can be shorter than that in the LTE system because of the subcarrier spacing (SCS) configurations. The LTE system has a fixed transmission unit due to a fixed frame structure and TTI length. Differing from the LTE system, the 5G system supports flexible numerology to set a slot as a basic dynamic scheduling unit and provide a flexible structure. Therefore, the TTI length is variable according to the SCS setting. In this simulation, we assume that SCS is 60 kHz. The transport block size of the 5G system is calculated using the formula in [35].

Unlike $N_{TBS,4G}$ in the LTE system, the transport block size of the 5G system, $N_{TBS,5G}$, is derived differently because of its broader bandwidth, various TTI lengths, and LDPC base graph. The $N_{TBS,5G}$ determination formula is derived according to the configured parameters, such as the code rate and data length. The detailed process is illustrated in [35]. Therefore, $N_{TBS,5G}$ can be defined as

$$N_{TBS,5G} = 8C \lceil \frac{N'_{info} + 24}{8C} \rceil - 24, \quad (8)$$

where C is $\lceil (N'_{info} + 24)/8424 \rceil$ and N'_{info} is the quantized intermediate number of information bits, which is expressed as

$$N'_{info} = 2^n \text{round}(\frac{N_{info} - 24}{2^n}), \quad (9)$$

where n is $\lfloor \log_2(N_{info} - 24) \rfloor - 5$, round($\cdot$) indicates the round function, and an unquantized intermediate variable, N_{info} is obtained as

$$N_{info} = RQ_m N_{RE}, \quad (10)$$

where R is the code rate and the number of the physical resource elements, N_{RE} is determined as

$$N_{RE} = \min(156, N'_{RE})n_{prb}, \quad (11)$$

where n_{prb} is the total number of allocated resource blocks and $N'_{RE} = N^{RB}_{SC} N^{sh}_{symb} - N^{PRB}_{DMRS} - N^{PRB}_{OH}$. N^{sh}_{symb} indicates the number of symbols within the slot in the 5G uplink, N^{PRB}_{DMRS} means the number of REs for demodulation reference signals (DM-RS) in the 5G uplink, and N^{PRB}_{OH} is the overhead
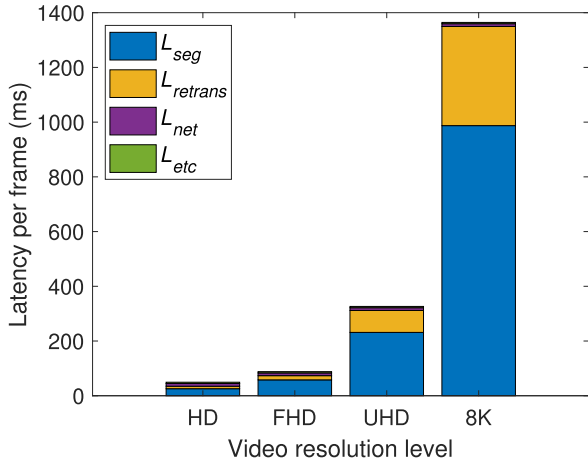
FIGURE 6. The end-to-end latency per frame of the raw video of the single user on the 5G system.

FIGURE 7. The end-to-end latency per frame of the encoded video of the single user on the 5G system.

FIGURE 8. The end-to-end latency per frame of the encoded FHD video of the single user on the 5G system with 50% background traffic.

configured by a higher layer parameter in the 5G uplink. Therefore, $L_{seg,5G}$ can be derived as

$$L_{seg,5G} = \lceil \frac{N_{video}}{N_{TBS,5G}} \rceil 2^{-\mu}, \qquad (12)$$

where μ is the numerology factor that allows flexible subcarrier spacing and symbol duration in the 5G system.

The retransmission latency in the 5G system, $L_{retrans,5G}$, is unsettled because of its flexible TTI length numerology. $T_{BS,HARQ}$ in the 5G system is

$$T_{BS,HARQ} = (N_1 + d_2)(2048 + 144)\kappa 2^{-\mu}T_c + T_{ext}, \quad (13)$$

where N_1 is the NACK processing time, which is defined from [35], T_c is the basic time unit in the 5G system, d_2 is the priority index parameter, κ is a constant that is set to 64, and T_{ext} is the time for operation with shared spectrum channel access. $T_{UE,HARQ}$ in the 5G system is defined as

$$T_{UE,HARQ} = (N_2 + d_2)(2048 + 144)\kappa 2^{mu}T_c + T_{ext} + T_{switch}, \qquad (14)$$

where N_2 is the uplink preparation time, which is illustrated in [35], and T_{switch} is the switching gap duration [33], [34], [35], [36]. In addition, T_{NACK} and T_{RT} are determined by the slot duration, $2^{-\mu}$, respectively.

Fig. 6 illustrates the end-to-end latency of each video frame of raw video of the single user under the 5G system. As shown in Fig. 2, L_T is still too large to support real-time video transmission even though using a higher modulation order and broader bandwidth in the 5G system can significantly reduce the end-to-end latency; specifically, L_T is approximately 362 ms and 50 ms under the 4G and 5G systems for FHD resolution, respectively. Therefore, the L_T of raw video transmission cannot satisfy the latency threshold, even in the 5G NR system. Additionally, similar to Fig. 2, L_{seg} and $L_{retrans}$ are the most dominant latency elements compared to other latency elements due to large data traffic in raw video transmission. Thus, to provide real-time video-sharing
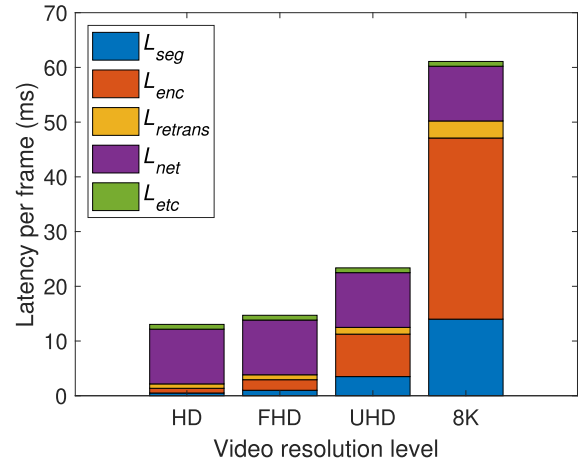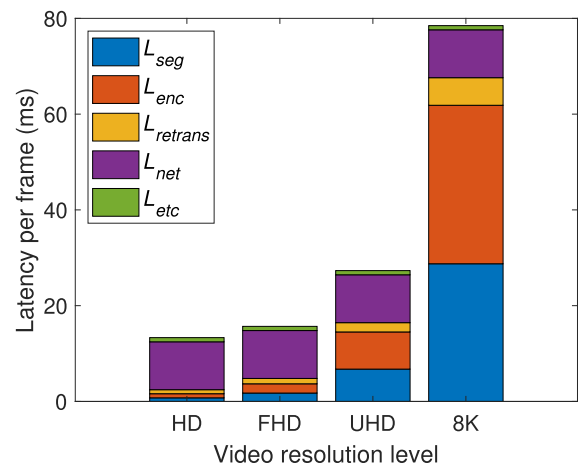
service with raw video, more advanced technologies that support wider bandwidth, higher modulation orders, and lower control overhead are needed, e.g., the 6G system.

Fig. 7 presents the end-to-end latency of the encoded video of the single user under the 5G system. Similar to the LTE system, as the video resolution level increases, L_T increases. Compared to the LTE system, the 5G system real-time video sharing system supports lower L_T; specifically, the 5G system supports 31.5% and 41.5% lower L_T in HD and FHD resolution levels compared to the LTE system, respectively. Additionally, in the 5G system, real-time video transmission with the encoded video can be supported up to UHD resolution due to a higher modulation order and broader bandwidth. Additionally, the TTI length is shorter in the 5G system because of the flexible numerology. Similar to the LTE system, at low video resolution levels, L_{net} and L_{etc} are the dominant latency elements. At high video resolution levels, L_{seg}, L_{enc}, and $L_{retrans}$ become the dominant latency elements. However, unlike the LTE system, L_{enc} greatly
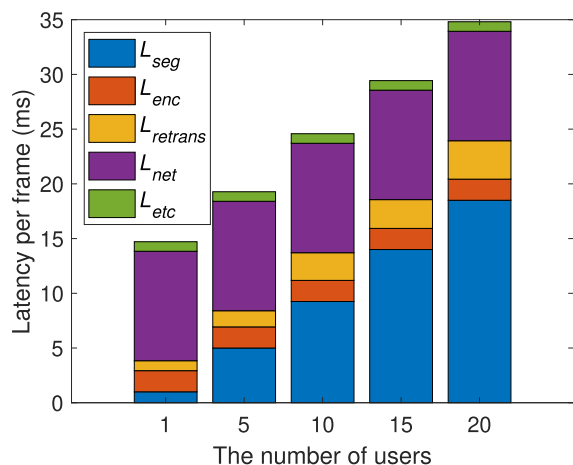
FIGURE 9. The end-to-end latency according to the number of users of encoded FHD video on the 5G system.

affects L_T at high video resolution levels because L_{seg} and $L_{retrans}$ are reduced due to the SCS configuration. Therefore, in 8K video resolution, L_{enc} becomes more dominant than other latency elements since L_{enc} does not change with the use of the 5G system, necessitating the use of fast encoding operations with advances in vision processing.

Fig. 8 illustrates the end-to-end latency per frame of the encoded video of the single user on the 5G system with 50% background traffic. Similar to Fig. 4, the latency performance in the 5G system under all resolution conditions shows degraded performance compared to the absence of background traffic. However, compared to LTE, the increase in the end-to-end latency was reduced because the 5G system supports more transmission block sizes than the LTE system. In addition, L_{seg} and $L_{retrans}$ decreased due to SCS configuration and reduced retransmission processing time, affecting end-to-end latency.

Fig. 9 displays the end-to-end latency of the encoded FHD video according to the number of users under the 5G system. As the number of users increases, L_T also increases because users should share limited resources. A real-time video-sharing service with FHD resolution under the 5G system can support up to 19 users, while only one user can be supported for the LTE system. Unlike the LTE system, the 5G system provides lower L_{seg} and $L_{retrans}$ since the TTI length can be reduced. In particular, in the LTE system, 8 ms latency occurs for each retransmission, but in the 5G system, approximately 1.2 ms latency for each retransmission occurs when using a 60 kHz SCS configuration due to the use of broader SCS and the reduction of processing latency, which are $L_{BS,HARQ}$ and $L_{UE,HARQ}$. Therefore, even though the number of frame segments and retransmissions is the same as those of the LTE system, lower L_{seg} and $L_{retrans}$ can be supported. Even in the 5G system, it is not enough to provide services to all vehicles on highways or urban environments when using real-time video-sharing services with FHD resolution. Therefore, the system should be provided for use cases that consider a limited number of vehicles as in LTE systems. To support more users, the service must be supported with low-resolution video or supported with larger bandwidth.

V. CONCLUSION

In this paper, we analyzed the end-to-end latency and latency elements per video frame for real-time video transmission services under LTE and 5G Uu interfaces. If the raw video is used for a real-time video-sharing system, it cannot be supported under both systems since the data traffic is too large to transmit within the latency threshold. In the LTE system, HD and FHD resolution levels can be supported with encoded video, and in the 5G system, resolution levels up to UHD can be supported. In the encoded video with a lower resolution level, network latency is dominant over the end-to-end latency per video frame because the required data traffic for each frame is low. However, with a high video resolution level, the segmentation latency and the retransmission latency dominate the end-to-end latency since higher data traffic needs to be supported. Additionally, we investigated the maximum number of users that can use a real-time video-sharing service with FHD resolution at the same time. In the LTE system, only a single user can be supported, but in the 5G system, it can support up to 19 users together due to broader bandwidth, SCS configuration, and higher modulation order. Compared to raw video, the encoded video has an additional encoding process latency. However, despite this additional encoding latency, it has more merit for the latency performance under the current system. If an advanced communication technology such as 6G is introduced and thus the end-to-end latency performance of raw video transmission can be improved, we can consider the trade-off with and without image encoding and decoding more seriously in terms of the latency as well as the frame quality.

REFERENCES

[1] A. Aijaz, "Private 5G: The future of industrial wireless," *IEEE Ind. Electron. Mag.*, vol. 14, no. 4, pp. 136–145, Dec. 2020.

[2] Y. Siriwardhana, G. Gür, M. Ylianttila, and M. Liyanage, "The role of 5G for digital healthcare against COVID-19 pandemic: Opportunities and challenges," *ICT Exp.*, vol. 7, no. 2, pp. 244–252, Jun. 2021.

[3] L. Banda, M. Mzyece, and F. Mekuria, "5G business models for mobile network operators—A survey," *IEEE Access*, vol. 10, pp. 94851–94886, 2022.

[4] R. Shrestha, S. Y. Nam, R. Bajracharya, and S. Kim, "Evolution of V2X communication and integration of blockchain for security enhancements," *Electronics*, vol. 9, no. 9, p. 1338, Aug. 2020.

[5] K. Z. Ghafoor, M. Guizani, L. Kong, H. S. Maghdid, and K. F. Jasim, "Enabling efficient coexistence of DSRC and C-V2X in vehicular networks," *IEEE Wireless Commun.*, vol. 27, no. 2, pp. 134–140, Apr. 2020.

[6] B. Sun and H. Zhang, *802.11 NGV Proposed PAR*, document IEEE 802.11-18/0861r9, 2018.

[7] *Architecture Enhancements for V2X Services*, document TS 23.285, Version 17.1.0, 3GPP, 2019.

[8] R. Kawasaki, H. Onishi, and T. Murase, "Performance evaluation on V2X communication with PC5-based and uu-based LTE in crash warning application," in *Proc. IEEE 6th Global Conf. Consum. Electron. (GCCE)*, Oct. 2017, pp. 1–2.

[9] J. Lianghai, A. Weinand, B. Han, and H. D. Schotten, "Multi-RATs support to improve V2X communication," in *Proc. IEEE Wireless Commun. Netw. Conf. (WCNC)*, Apr. 2018, pp. 1–6.

[10] *Service Requirements for Enhanced V2X Scenarios*, document TR 22.18, Version 16.2.0, 3GPP, 2020.

[11] A. Festag, "Cooperative intelligent transport systems standards in Europe," *IEEE Commun. Mag.*, vol. 52, no. 12, pp. 166–172, Dec. 2014.

[12] R. Weber, J. Misener, and V. Park, "C-V2X—A communication technology for cooperative, connected and automated mobility," in *Proc. Mobile Commun. Technol. Appl., ITG-Symp.*, 2019, pp. 1–6.

[13] M. Wang, M. Winbjork, Z. Zhang, R. Blasco, H. Do, S. Sorrentino, M. Belleschi, and Y. Zang, "Comparison of LTE and DSRC-based connectivity for intelligent transportation systems," in *Proc. IEEE 85th Veh. Technol. Conf. (VTC Spring)*, Jun. 2017, pp. 1–5.

[14] *C-V2X Use Cases, Methodology, Examples and Service Level Requirements*, 5GAA, Munich, Germany, 2021.

[15] K. Moto, M. Mikami, K. Serizawa, and H. Yoshino, "Field experimental evaluation on 5G V2N low latency communication for application to truck platooning," in *Proc. IEEE 90th Veh. Technol. Conf. (VTC-Fall)*, Sep. 2019, pp. 1–5.

[16] R. Liu, D. Kwak, S. Devarakonda, K. Bekris, and L. Iftode, "Investigating remote driving over the LTE network," in *Proc. 9th Int. Conf. Automot. User Interfaces Interact. Veh. Appl.*, Sep. 2017, pp. 264–269.

[17] Z. Tan, J. Zhao, Y. Li, Y. Xu, and S. Lu, "Device-based LTE latency reduction at the application layer," in *Proc. 18th USENIX Symp. Netw. Syst. Design Implement. (NSDI)*, 2021, pp. 471–486.

[18] J.-M. Georg, J. Feiler, S. Hoffmann, and F. Diermeyer, "Sensor and actuator latency during teleoperation of automated vehicles," in *Proc. IEEE Intell. Vehicles Symp. (IV)*, Oct. 2020, pp. 760–766.

[19] B. Coll-Perales, M. C. Lucas-Estañ, T. Shimizu, J. Gozálvez, T. Higuchi, S. Avedisov, O. Altintas, and M. Sepulcre, "End-to-end V2X latency modeling and analysis in 5G networks," 2022, *arXiv:2201.06082*.

[20] M. C. Lucas-Estañ, B. Coll-Perales, T. Shimizu, J. Gozálvez, T. Higuchi, S. Avedisov, O. Altintas, and M. Sepulcre, "An analytical latency model and evaluation of the capacity of 5G NR to support V2X services using V2N2V communications," 2022, *arXiv:2201.06083*.

[21] K. Lee, J. Kim, Y. Park, H. Wang, and D. Hong, "Latency of cellular-based V2X: Perspectives on TTI-proportional latency and TTI-independent latency," *IEEE Access*, vol. 5, pp. 15800–15809, 2017.

[22] S. A. Ashraf, I. Aktas, E. Eriksson, K. W. Helmersson, and J. Ansari, "Ultra-reliable and low-latency communication for wireless factory automation: From LTE to 5G," in *Proc. IEEE 21st Int. Conf. Emerg. Technol. Factory Autom. (ETFA)*, Sep. 2016, pp. 1–8.

[23] P. V. Grammatikos and P. G. Cottis, "A mobile edge computing approach for vehicle to everything communications," *Commun. Netw.*, vol. 11, no. 3, pp. 65–81, 2019.

[24] *Study on LTE-Based V2X Services*, document TR 36.885, Version 14.0.0, 2016.

[25] *Evolved Universal Terrestrial Radio Access (E-UTRA); Study on Group Communication for E-UTRA*, document TR 36.868, Version 12.0.0, 3GPP, 2014.

[26] Y. Tew and K. Wong, "An overview of information hiding in H.264/AVC compressed video," *IEEE Trans. Circuits Syst. Video Technol.*, vol. 24, no. 2, pp. 305–319, Feb. 2014.

[27] *Series H: Audiovisual and Multimedia Systems; Infrastructure of Audiovisual Services—Coding of Moving Video*, ITU-T, Geneva, Switzerland, Version 12, 2017.

[28] G. J. Sullivan, J.-R. Ohm, W.-J. Han, and T. Wiegand, "Overview of the high efficiency video coding (HEVC) standard," *IEEE Trans. Circuits Syst. Video Technol.*, vol. 22, no. 12, pp. 1649–1668, Dec. 2012.

[29] B. Sklar, "A primer on turbo code concepts," *IEEE Commun. Mag.*, vol. 35, no. 12, pp. 94–102, Dec. 1997.

[30] *Evolved Universal Terrestrial Radio Access (E-UTRA); Physical Layer Procedures*, document TS 36.213, Version 14.2.0, 3GPP, 2017.

[31] *Study on Channel Model for Frequencies From 0.5 to 100 GHz*, document TR 38.901, Version 16.1.0, 3GPP, 2020.

[32] *Study on Evaluation Methodology of New Vehicle-to-Everything (V2X) Use Cases for LTE and NR*, document TR 37.885, Version 15.3.0, 3GPP, 2019.

[33] *Study on Self Evaluation Towards IMT-2020 Submission*, document TR 37.910, Version 16.1.0, 3GPP, 2020.

[34] D. Hui, S. Sandberg, Y. Blankenship, M. Andersson, and L. Grosjean, "Channel coding in 5G new radio: A tutorial overview and performance comparison with 4G LTE," *IEEE Veh. Technol. Mag.*, vol. 13, no. 4, pp. 60–69, Dec. 2018.

[35] *Physical Layer Procedures for Data*, document TS 38.214, Version 15.3.0, 3GPP, 2020.

[36] *Physical Channels and Modulation*, document TS 38.211, Version 16.2.0, 3GPP, 2020.

SINUK CHOI received the B.S. degree in electronics engineering from Kyungpook National University, Daegu, South Korea, in 2017. He is currently pursuing the Ph.D. degree with the Department of Electrical Engineering and Computer Science, Daegu Gyeongbuk Institute of Science and Technology, Daegu. His research interests include vehicle-to-everything communication and cellular communication systems.

DONGYOON KWON received the B.S. degree in electronic engineering from Kyungsung University, Busan, South Korea, in 2021. He is currently pursuing the M.S. degree with the Department of Electrical Engineering and Computer Science, Daegu Gyeongbuk Institute of Science and Technology, Daegu, South Korea. His research interests include vehicle-to-everything communication and autonomous driving.

JI-WOONG CHOI (Senior Member, IEEE) received the B.S., M.S., and Ph.D. degrees from Seoul National University (SNU), Seoul, South Korea, in 1998, 2000, and 2004, respectively, all in electrical engineering. From 2004 to 2005, he was a Postdoctoral Researcher with the Inter-University Semiconductor Research Center, SNU. From 2005 to 2007, he was a Postdoctoral Visiting Scholar with the Department of Electrical Engineering, Stanford University, Stanford, CA, USA. He was also a Consultant with GCT Semiconductor, San Jose, CA, USA, for the development of mobile TV receivers, from 2006 to 2007. From 2007 to 2010, he was with Marvell Semiconductor, Santa Clara, CA, USA, as a Staff Systems Engineer for next-generation wireless communication systems, including WiMAX and LTE. Since 2010, he has been a Professor with the Department of Electrical Engineering and Computer Science, Daegu Gyeongbuk Institute of Science and Technology (DGIST), Daegu, South Korea. His research interests include wireless communication theory, signal processing, biomedical communication applications, and brain–machine interface.

● ● ●